Atmospheric Environment 207 (2019) 16–29

Contents lists available at ScienceDirect

Atmospheric Environment

journal homepage: www.elsevier.com/locate/atmosenv

Sensitivity of simulating a dust storm over Central Asia to different dust schemes using the WRF-Chem model

Tiangang Yuan, Siyu Chen*, Jianping Huang*, Xiaorui Zhang, Yuan Luo, Xiaojun Ma, Guolong Zhang

Key Laboratory for Semi-Arid Climate Change of the Ministry of Education, Lanzhou University, Lanzhou, 730000, China

ARTICLE INFO

Keywords:
Central Asia
WRF-Chem
Dust emission schemes
Threshold friction velocity

ABSTRACT

Frequent dust storms have harm to human health and agricultural activities in Central Asia. However, there has been a great deal of uncertainty in prediction of dust storms in Central Asia. One of the important reasons is that the adaptability of different dust emission schemes has not been evaluated. Here, the Goddard Chemistry Aerosol Radiation and Transport (GOCART), Air Force Weather Agency (AFWA) and Shao2004 (Shao04) dust schemes coupled to the WRF-Chem model were used to simulate the severe dust storm occurred in Central Asia on 12–15 July 2016. Generally, this dust storm was initialed by a vortex at 500 hPa and surface cold front, and then swept across Turkmenistan, Uzbekistan and Tajikistan. The Shao04 case could represent the spatial-temporal evolution of the dust storm well, especially at the northern Iran and Turkmenistan, due to its better description of the physical process of dust emission. But it overestimated the aerosol optical depth (AOD) to the southeast of the Aral Sea, which might be associated with the uncertainties of the soil particle distribution dataset. The AFWA case simulated AOD as better as Shao04 case with improved soil moisture correction factors, saltation algorithms and particle size distributions although it had smaller particle size, indicating that smaller particles are assignable. The GOCART case showed the largest dust emission areas due to the low threshold velocity. Yet both the AFWA and GOCART scheme underestimated the high AOD over northern Iran owe to its low erodibility factors. The total dust emission of the four-day period in the Shao04 scheme was 11.9 Tg, which was 2–3 times larger than those obtained in the AFWA and GOCART schemes. The significant differences of dust emission between three dust schemes may essentially depend on the sensitivities of threshold friction velocity on surface property.

1. Introduction

Dust aerosols, as major components of tropospheric aerosols, are mainly derived from wind erosion in arid and semi-arid regions (Huang et al., 2007, 2017; Zhao et al., 2013). Dust particles can significantly heat the atmosphere by absorbing solar radiation (Chen et al., 2017a; Zhang et al., 2013; Wu et al., 2013; Han et al., 2012), and they can also change the optical properties and lifespans of clouds by acting as condensation nuclei and ice cores, which further affect weather and climate systems (Shao et al., 2011a; Guo and Yin, 2015; Huang et al., 2014). Moreover, the long-term transport of dust aerosols provides nutritive material (such as iron) for marine organisms, thus enhancing the biological pump, which in turn reduces global warming by decreasing the CO_2 in the atmosphere (Wang et al., 2012, 2017). In addition, the long-term transport can also enhance soil salinization (Popov, 1998), change the efficiency of photosynthesis (Usmanov, 1998; Shao et al., 2011a) and accelerate chemical reactions (Kameda et al., 2016).

Central Asia is located in the center of global dust belt, where the strong wind speed, low vegetation coverage and frequent drought conditions, especially in the context of global warming, contribute more to the expansion of drylands and increase in dust storms (Huang et al., 2015a, 2016; 2017; Rashki et al., 2018; Wang et al., 2017). It is generally confirmed that the Kyzylkum, Karakum, Aralkum and Balkhash regions in Central Asia have been the major dust source regions since dust storms began to be monitored in 1936 (Orlovsky et al., 2005; Middleton, 2017; Indoitu et al., 2012; Groll et al., 2013). The dust storms over Central Asia have significant impacts on human health and social and economic development due to their long-distance transport, mixing with anthropogenic pollutants and low visibility (Prospero, 1999; Opp, 2005; Abuduwaili et al., 2010; Hofer et al., 2017). Sternberg and Edwards (2017) reviewed the dust storms occurring in Central Asia and their impacts on health and found that the dust originated from

* Corresponding authors.
E-mail addresses: chensiyu@lzu.edu.cn (S. Chen), hjp@lzu.edu.cn (J. Huang).

https://doi.org/10.1016/j.atmosenv.2019.03.014
Received 9 November 2018; Received in revised form 9 March 2019; Accepted 16 March 2019
Available online 20 March 2019
1352-2310/

Kyzykum, Karakum, Aralkum, and Balkash can lead to respiratory ailments, lung disease, eye and throat aliments, and meningitis, respectively under human activities. Moreover, the salinization process of soils and degradation of vegetation can be intensified by dust storms, which can further reduce the production of crops over Central Asia (Ochmann and Nowak, 2009; Orlovsky et al., 2004; Indoitu et al., 2012; Opp et al., 2017).

Therefore, accurate forecasting and modeling of dust storms is significant for reducing economic loss and human injury in Central Asia. Since the dust emission is highly dependent on surface properties, dust schemes have been proposed by previous studies (e.g., Ginoux et al., 2001; Shao, 2004; Shao et al., 2011b). It remains challenging to estimate dust emission using different dust schemes especially in regional models (Tanaka and Chiba, 2006; Textor et al., 2006; Huneeus et al., 2011; Zhao et al., 2013; Chen et al., 2017a). Zhao et al. (2010) compared the performances of the Goddard Chemistry Aerosol Radiation and Transport (GOCART) and DUST TRANsport model (DUSTRAN) dust schemes and found that the DUSTRAN scheme overestimated dust emission over the west coast of North Africa. Wu and Lin (2014) found that the Shao04 dust scheme (Shao, 2004) is capable of simulating dust emission and transport and that GOCART ignored potential dust sources in parts of Mongolia over East Asia. Su and Fung (2015) further pointed out that the Air Force Weather Agency (AFWA) dust schemes omit the dust emission in the Gobi Desert over East Asia and that the Shao11 dust scheme (Shao et al., 2011b) has a better performance. The better performance of the Shao dust scheme mainly owes to its better description of the physical process of dust emission (Shao et al., 2011b).

Nevertheless, there has been a great deal of uncertainty in the prediction of dust storms in Central Asia. One of the important reasons is that the adaptability of different dust emission schemes has not yet been evaluated here. What about the sensitivities of different dust scheme in this region? Which dust scheme can better describe the process of dust storm? Since the GOCART, AFWA, and Shao04 dust schemes have been coupled to the WRF-Chem model, this paper systematically compared the performances of the three dust schemes in dust modeling using the WRF-Chem model to obtain an optimal dust scheme for Central Asia based on a dust storm that occurred on 12–15 July 2016. The results in this paper can be used as a reference for dust storm modeling and forecasting in Central Asia.

This paper is structured as follows. The three dust schemes and WRF-Chem model configuration are described in section 2. Section 3 shows the in situ measurements and satellite observations used in this paper. The model evaluation and results are illustrated in section 4. Conclusion and discussion are demonstrated in section 5.

2. Model description and dust emission schemes

The Weather Research and Forecasting (WRF) model is a mesoscale numerical weather prediction system designed for both atmospheric research and operational forecasting applications; it covers a wide range of meteorological applications across scales ranging from tens of meters to thousands of kilometers (https://www.mmm.ucar.edu/weather-research-and-forecasting-model). The WRF coupled with an atmospheric chemistry module, i.e., the WRF-Chem model, is an air quality model that includes photolysis schemes, gas-phase chemical mechanisms, and aerosol schemes by considering a variety of coupled physical and chemical processes, such as aerosol emission and transport (i.e., advection, diffusion, and convection), dry/wet deposition, chemical processes, aerosol interactions, and the energy budget (Grell et al., 2005). The online coupling of meteorology and chemistry in the WRF-Chem model can be used to accurately represent the evolution of trace gases and aerosols, which can demonstrate the feedbacks between aerosols and meteorological fields better than other offline models (Fast et al., 2006). In this paper, the WRF-Chem model version 3.8.1 was used to investigate the sensitivity of WRF-Chem model to differennt dust schemes over Central Asia.

Table 1
Fractions of five dust size bins in GOCART and AFWA.

Type	Particle size (μm)	GOCART	AFWA
Bin1	0–1	0.1	0.1074
Bin2	1–1.8	0.25	0.1012
Bin3	1.8–3	0.25	0.2078
Bin4	3–6	0.25	0.4817
Bin5	6–10	0.25	0.1019

2.1. GOCART dust scheme

The GOCART scheme calculates vertical dust flux in five size bins and uses 10 m wind speed and soil wetness (Ginoux et al., 2001). The vertical dust flux (G, μg m^{-2} s^{-1}) at each size bin is determined by

$$G = CSs_p u_{10m}^2 (u_{10m} - u_t),\ u_{10m} > u_{10t}, \quad (1)$$

where C is an empirical proportionality constant that is set here as 0.8 μg s^{-2} m^5; S is the erodibility function which defines the potential dust source regions and comprises surface factors, such as snow cover and vegetation; s_p is the fraction of each size class; u_{10m} is the horizontal wind speed at 10 m; u_{10t} is the threshold velocity, which is a function of soil wetness, particle size and air density. Five bins of dust particles treated in GOCART scheme are 0–1 μm, 1–1.8 μm, 1.8–3 μm, 3–6 μm, 6–10 μm in WRF-Chem. The fractions in the five dust bins are shown in Table 1. On the basis of Eq. (1), we can conclude that the G is closely related to the particles size distribution, u_{10t} and erodibility. The GOCART scheme has been used to model dust storms over North Africa, North America and East Asia and shows good performance (Zhao et al., 2010, 2011, 2013; Chen et al., 2013, 2017b, 2018).

2.2. AFWA dust scheme

The AFWA dust scheme (Jones et al., 2010, 2012) was developed from the work of Marticorena and Bergametti (1995), who considered the dust particles produced from the saltation bombardment process. The dust flux is calculated as

$$H(D_p) = C\frac{\rho_a}{g}u_*^3\left(1 + \frac{u_{*t}}{u_*}\right)\left(1 - \frac{u_{*t}^2}{u_*^2}\right), \quad (2)$$

$$G = \sum H(D_p) dS_{rel}(D_p), \quad (3)$$

$$F_{bulk} = G\alpha \times S, \quad (4)$$

$$\alpha = 10^{0.136(\%clay)-6}, \quad (5)$$

where $H(D_p)$ is the saltation flux; C is the emission factor constant, which is set as 1; ρ_a is the air density; g is gravitational acceleration; u_* is the friction velocity and u_{*t} is the threshold friction velocity; G is the sum of each particle size bombardment; F_{bulk} is the vertical dust flux; S is the erodibility function and α is the bombardment efficiency factor (Gillette, 1979). This scheme firstly calculates the saltation flux with large effective particle size ranging from 0.71 to 125 μm according to Eqs. (2) and (3), and then calculates the vertical dust flux of all bins using Eq. (4) based on Marticorena and Bergametti (1995). It should be noted that Marticorena and Bergametti only provided the total vertical dust emission, and dust flux in different particle sizes is not clear. Kok (2011)developed particle sizes distribution in view of Brittle Materials Fragmentation Theory and the fraction of five size distributions are illustrated in Table 1 with the same effective particle sizes as GOCART scheme. Thus, vertical dust flux in different size bins can be obtained through redistributing the total dust emission with new particle size distribution. Besides, AFWA uses friction velocity (u_*) and threshold friction velocity (u_{*t}) instead of wind speed at 10 m. The u_{*t} tends to increase if soil moisture greater than dry limit and is treated as dry (no correction) when soil moisture less than dry limit. Overall, the AFWA

scheme has been greatly improved in terms of its soil moisture correction factors, saltation algorithms and particle size distributions compare to GOCART scheme.

2.3. Shao04 dust scheme

Shao (2004) proposed a size-resolved dust scheme (hereafter referred to as Shao04) that takes the bombardment and aggregate disintegration of particles into account. The performance of the Shao04 scheme was tested with the Japan-Australia Dust Experiment by Shao et al. (2011b), and the estimated dust flux generally agreed well with the observations. The Shao04 scheme is as follows:

$$F(d_i, d_s) = c_y \eta_{fi} \sigma_p [(1-\gamma) + \gamma \sigma_p](1+\sigma_m) g \frac{Q_{ds}}{u_*^2}, \tag{6}$$

$$F(d_i) = \int_{d_1}^{d_2} F(d_i, d_s) p_s(d) \delta d, \tag{7}$$

$$p_s(d) = \gamma p_m(d) + (1-\gamma) p_f(d), \tag{8}$$

$$G = \sum_i F(d_i), \tag{9}$$

$$d \times p(d) = \sum_{j=1}^{N} \frac{w_j}{\sqrt{2\pi}\sigma_j} \exp\left[-\frac{(\ln d - \ln D)^2}{2\sigma_j^2}\right], \tag{10}$$

where $F(d_i,d_s)$ is the vertical dust flux of particle size d_i induced by the saltation of particle d_s; c_y is the proportionality factor; η_{fi} is the fraction of dust emitted; σ_p is the mass ratio of free and aggregated dust; σ_m is the bombardment efficiency; γ describes the ability of aggregated dust to be released; Q_{ds} is the saltation flux of particles d_s; $F(d_i)$ is the total dust flux of the particle size di from the saltation of all grain sizes between d_1 and d_2; G is the total vertical dust flux of all particle sizes; w_j is the weight for the jth mode of particle size distribution; σ_j and Dj are used for the lognormal distribution of the jth mode. $p_m(d)$ and $p_f(d)$ is the minimally and fully distributed particle size distribution of the parent soil, respectively. Both $p_m(d)$ and $p_f(d)$ are mainly used to constrain the size distribution of sand and dust particles, $p_s(d)$. Thus, the adaptability of the Shao04 scheme in calculating the size resolved dust flux depends on the accuracy of parent soil data and γ. Similar to AFWA, the Shao04 scheme also calculates the vertical dust flux using sandblasting parameterization. In the Shao04 scheme, dust particles firstly are divided into 100 classes with max particles size of 2000 μm to calculate the minimally, fully particle size distribution according to Eq. (10). Then the vertical dust flux at each size class is also available with Eq. (6) – (8). Subsequently, size cut diameter is designed as 2 μm, 3.6 μm, 6 μm, 12 μm, and 20 μm. Therefore, vertical dust emission flux at each interval (0–2 μm, 2–3.6 μm, 3.6–6 μm, 6–12 μm and 12–20 μm) will be calculated. Different with the AFWA and GOCART scheme, the Shao04 scheme only uses erodibility factors to constrain the potential emission areas.

2.4. Numerical experiment configuration

The Morrison two-moment microphysical scheme (Morrison et al., 2005), Kain-Fritsch cumulus convection scheme (Kain and Fritsch, 1990; Kain, 2004), Yonsei University (YSU) planetary boundary layer scheme (Hong et al., 2006), Noah land-surface mode (Chen et al., 1996; Chen and Dudhia, 2001), Revised MM5 surface layer scheme (Jimenez et al., 2012), Rapid radiative transfer model (RRTMG) (Mlawer et al., 1997; Iacono et al., 2000) for longwave and shortwave radiation are used in this paper. The aerosol feedback to meteorological field is also included, which will make it closer to the real atmosphere. The GOCART aerosol chemistry model can simulate dust, sea salt, sulfate, the hydrophobic and hydrophilic black carbon and organic carbon (Chin et al., 2000). Among of which, the dust, hydrophobic and hydrophilic

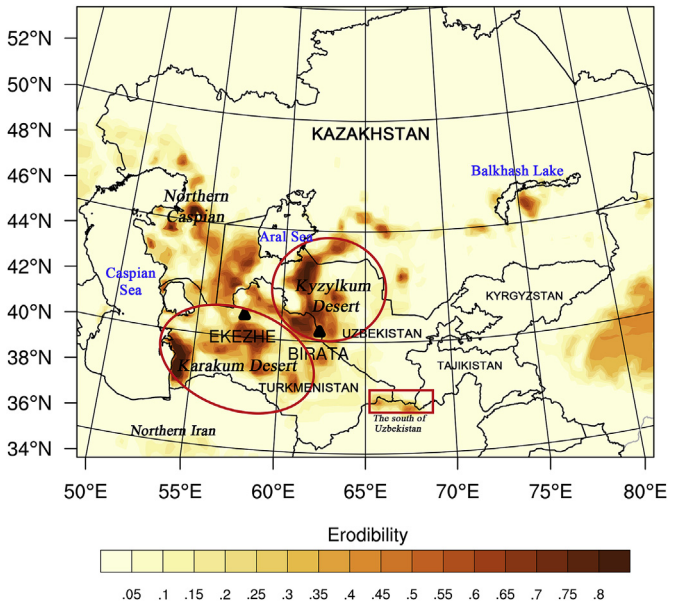

Fig. 1. Model domain and spatial distribution of the erodibility factor used in GOCART and AFWA dust schemes. (Red box and ellipses are major deserts; two triangles are the locations of the EKEZHE and BIRATA weather stations). (For interpretation of the references to color in this figure legend, the reader is referred to the Web version of this article.)

black carbon and organic carbon are considered in this study using the Emissions Database for Global Atmospheric Research – Hemispheric Transport of Air Pollution (EDGAR-HTAP). The study domain covers Central Asia, including Kazakhstan, Turkmenistan, Uzbekistan, Kyrgyzstan and Tajikistan, with grid cells of 147 × 188, which are shown (along with erodibility data) in Fig. 1. The dust source region mainly includes the northern Caspian, Karakum desert, Kyzylkum desert, the southern region of the Balkhash Lake and some of the Aral region. Due to the complexity of wet deposition and dominant dry deposition over Central Asia, only dry deposition was considered in this paper. The horizontal resolution is 15 km and the pressure in the top of atmosphere is 100 hPa in this experiment. The National Center for Environmental Prediction Final Analysis (NCEP/FNL), with a temporal interval of 6 h and a horizontal resolution of 1° × 1°, was used to provide the initial and boundary conditions for the model. The model configurations in the three simulations are treated the same except for the consideration of different dust emission schemes. The dust storm studied here occurred in Central Asia from 12 to 15 July 2016; therefore, this time period (hereafter referred to as the simulation period) was simulated with time step of 90 s and frequency of output every three hours.

3. Observations

3.1. Meteorology

The NCEP/FNL Reanalysis data were used to analyze the synoptic process. The daily average wind speed at 10 m and temperature at 2 m obtained from 176 meteorological stations from the National Oceanic and Atmospheric Administration (NOAA) - National Climatic Data Center Surface (NCDC) were used to evaluate the performance of the WRF-Chem on meteorological fields. Moreover, the wind field, air temperature and pressure from the China Meteorological Administration with 3 h interval at the weather station of EKEZHE and BIRATA near the Kyzylkum and Karakum deserts were selected to demonstrate the diurnal variation of meteorological elements.

3.2. Satellite datasets

To clearly demonstrate the evolution of the simulated dust storm, Moderate-resolution Imaging Spectroradiometer (MODIS) True color images on Aqua were used. The aerosol optical depth (AOD) data retrieved by MODIS on Aqua were used to evaluate the simulated aerosols. MODIS has a wide coverage, wide band (0.12–14.24 μm) and high spectral resolution, and it can provide information about land, atmosphere, clouds, and aerosols. Compared with the Dark Target algorithm, the Deep Blue algorithm uses the blue channel to obtain the optical properties of aerosols with high surface albedo, such as those in deserts and snow surfaces (Hsu et al., 2006, 2013). In the enhanced Deep Blue products, a number of pixels have achieved QA = 2 and 3 compared with Collection 5, which can reduce the effect of clouds through QA (Hsu et al., 2013). Therefore, the Collection 6 Level-2 MODIS Deep Blue (DB) AOD products on Aqua (MYD04_L2), with a temporal resolution of 5 min and a spatial resolution of 10 km, were used in this paper. Because different time period and coverage will affect the model evaluation, we subsample the model output AOD to match the MODIS time period and coverage. The Cloud Aerosol Lidar with Orthogonal Polarization (CALIOP) on Cloud-Aerosol Lidar and Infrared Pathfinder Satellite Observations (CALIPSO) can accurately detect various types of aerosols, such as smoke, pure dust, and polluted dust (Chen et al., 2010; Huang et al., 2015b). It can also provide attenuated backscatter, aerosol extinction coefficients at 1064 nm and 532 nm, and column AOD data at the troposphere and stratosphere (Vaughan et al., 2004; Winker et al., 2003). The products of Level 2 on 21 UTC 13 July 2016 were used to display the vertical structures of aerosols.

4. Results

4.1. Comparison of meteorological conditions

Dust emission process is closely related to meteorological elements such as wind speed, temperature and soil moisture. Fig. 2 shows the comparison of the average temperature at 2 m and wind speed at 10 m between the model results and station observations during the simulation period. Generally, the spatial patterns of the deviation of temperature and wind speed are aligned with the distribution of terrain in Central Asia. The terrain in Central Asia is generally low in the northwest and high in the southeast. Therefore, the large deviations of wind speed and temperature mainly appear at the Tianshan Mountains and Pamir Plateau because of the coarse model resolution. Over flat areas, ground stations tend to be more representative of the model grids. As for average temperature at 2 m, the model generally overestimates it over flat areas with error less than 3 °C and underestimates it over complex terrain (southeast of the domain) with error more than 5 °C (Fig. 2a). The errors of average of wind speed are smaller than that of temperature over flat areas. And the wind speed is only slightly overestimated at Mountain regions (Fig. 2c). In addition, the regional average temperature (wind speed) determined from observations and the WRF-Chem model are 26.0 °C (3.5 m s^{-1}) and 26.4 °C (3.4 m s^{-1}), respectively. Stations with errors within 2 °C (m s^{-1}) and 4 °C (m s^{-1}) accounted for 63% (81%) and 92% (95%), respectively, of all stations, and the root mean square error (RMSE) was 3.19 °C (1.39 m s^{-1}). On the whole, the simulated average wind speed and temperature are in accord with in situ measurements.

To gain more insight, the four-day variations of wind speed and temperature observed by the BIRATA and EKEZHE stations located near deserts and the corresponding model results are shown in Fig. 3. The WRF-Chem model captures the diurnal change of meteorological elements well, especially for air temperature at 2 m. The correlation coefficients between the observed and simulated wind speed, temperature and pressure are as high as 0.72–0.73, 0.9–0.94 and 0.94–0.95 with a significance of 95% and a small RMSE, respectively. However, the model generally overestimates the wind speed at 10 m, especially the strong winds. This is a common issue in the WRF model simulations, which may be caused by the existence of errors in the initial field of NCEP/FNL, or the limitations in simulating the turbulence processes and sub-grid scale parameterizations (Hanna et al., 2000). Moreover, the simulation of wind speed may have large uncertainty and strong sensitivity to the applied physics parameterizations, particularly to

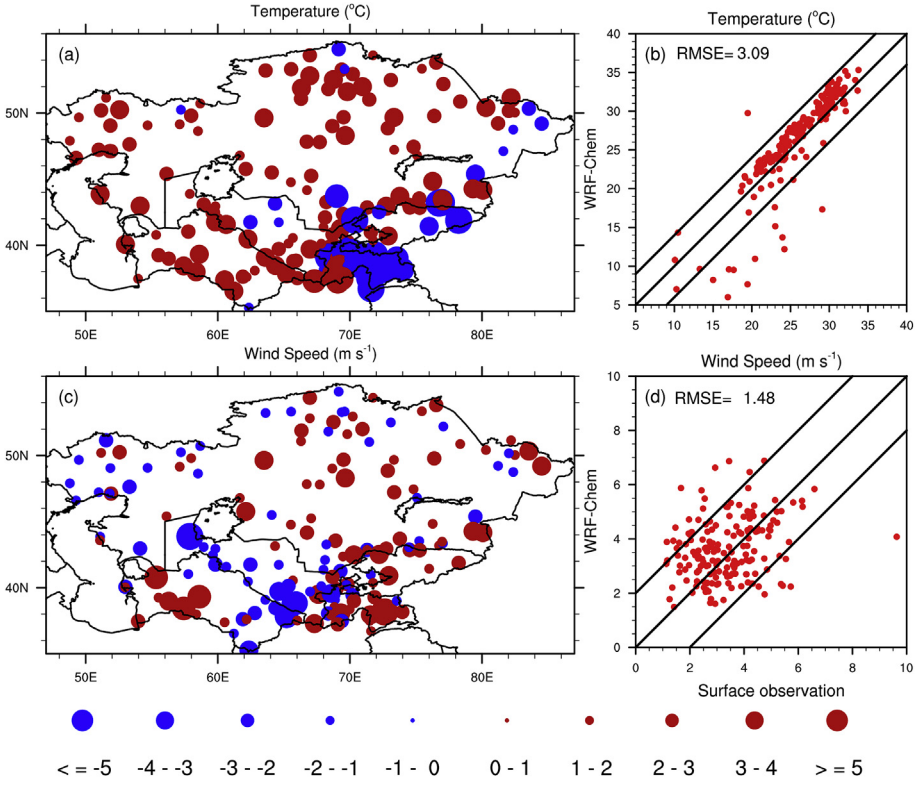

Fig. 2. Comparison of four-day average (a, b) temperature at 2 m (°C) and (c, d) wind speed at 10 m (m s^{-1}) between model results and station observations from 12 to 15 July.(Left panel shows the difference of model results subtract observations; right panel shows the variation of model results and observations at weather stations).

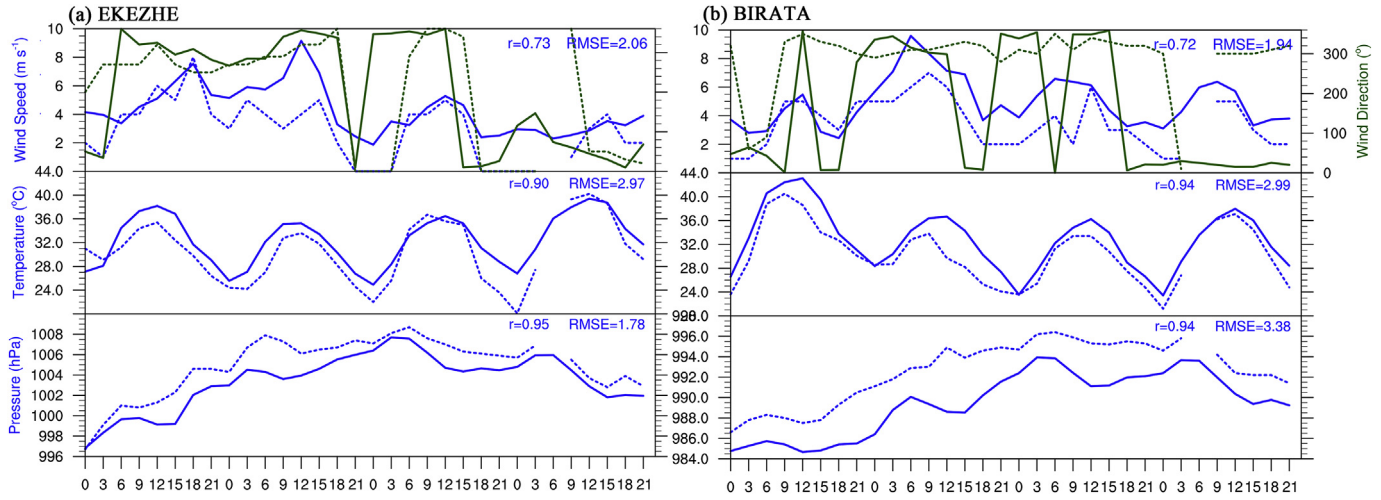

Fig. 3. Diurnal changes of meteorological elements from model results and station observations at (a) EKEZHE and (b) BIRATA. Top panel is the wind speed (blue lines, m s^{-1}) and wind direction (green lines, °) at 10 m; middle panel is temperature at 2 m (°C); bottom panel is surface pressure (hPa). (The solid and dashed lines represent simulations and observations, respectively, and their corresponding correlation coefficients (r) and root mean square error (RMSE) values are shown in right corners). (For interpretation of the references to color in this figure legend, the reader is referred to the Web version of this article.)

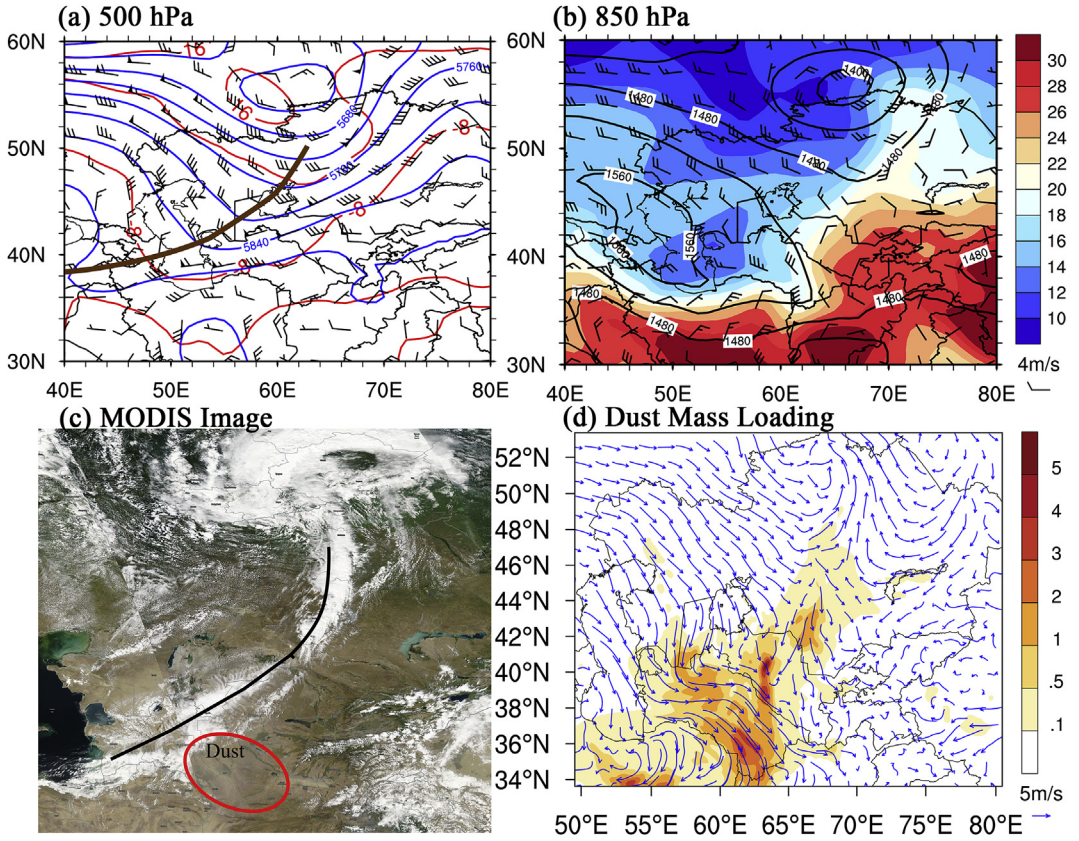

Fig. 4. Spatial distributions of geopotential height (blue contour lines, units: gpm), temperature (red contour lines, units: °C) and wind field (vectors) at (a) 500 hPa and (b) 850 hPa (color filling is temperature (°C)) from NCEP/FNL reanalysis data, (c) MODIS image on Aqua and (d) dust mass loading (g m^{-2}) from WRF-Chem model using AFWA dust scheme at 06 UTC on 13 July. Red circles represent dust areas. (For interpretation of the references to color in this figure legend, the reader is referred to the Web version of this article.)

those related to the planetary boundary layer and surface-layer processes (Yang et al., 2017). Although the model overestimates the wind speed, the diurnal variation of wind speed is captured by the model. Thus, the dust emission flux may be overestimated but the spatial and temporal distribution of dust lifting will not be affected. To decrease the uncertainties of dust emission flux caused by wind speed in dust source regions, the dust emission factor C in the dust schemes can be adjusted to compensate the overestimation of wind speed (Chen et al., 2014). Besides, the process of the cold front across the Karakum and Kyzylkum deserts are also depicted by the change of meteorological field remarkably. Both stations exhibit positive pressure changes and negative temperature changes from 12 to 13 July, indicating that the cold front reached the Karakum and Kyzylkum deserts. Moreover, the wind direction turns northerly, and the maximum temperature dropped by

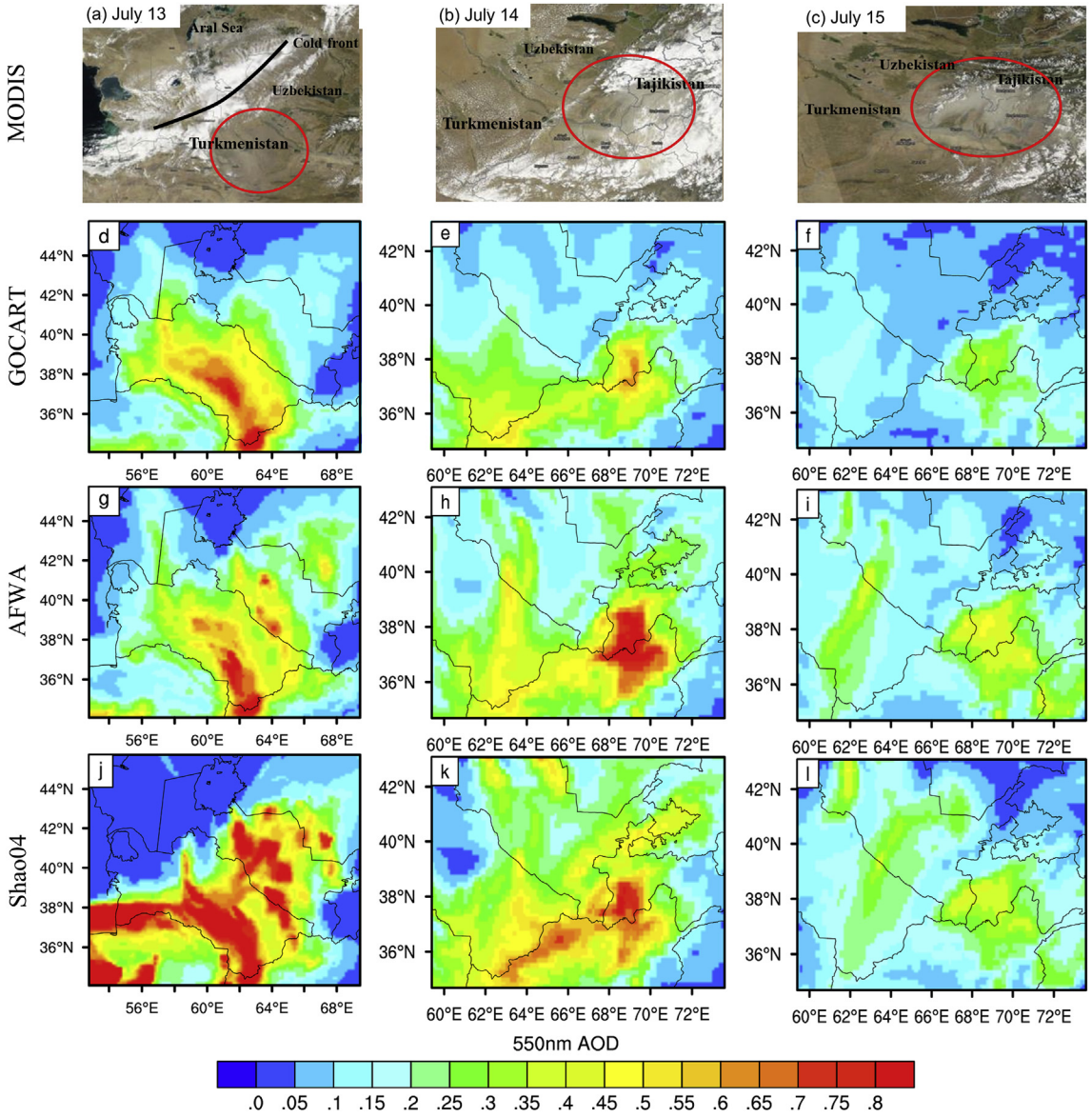

Fig. 5. The dust layers detected by (a–c) MODIS on Aqua red-green-blue color composite images and the corresponding simulated AOD at 550 nm from (d–f) GOCART, (g–i) AFWA and (j–l) Shao04 dust schemes on 13 to 15 July 2016. (Black line is the cold front; red circles represent dust areas.). (For interpretation of the references to color in this figure legend, the reader is referred to the Web version of this article.)

approximately 8 °C. After 14 July, with the decreased station pressure and increased temperature, the cold front passed the dust source regions. Compared with the observations, the model only slightly underestimates the air pressure and overestimates the temperature. Overall, the WRF-Chem model could capture the temporal and spatial variations of meteorological elements well, which provides more confidence for further investigating dust emission and transport processes.

4.2. Synoptic processes and simulated dust storm

The dust storm was closely associated with the vortex trough at 500 hPa and the surface cold front (Fig. 4). A deep cold vortex was formed at 500 hPa over the northern Kazakhstan, and the trough extended southwest towards northern Iran at 06 UTC on 13 July. Strong cold air stretched from the North Pole to Central Asia by strong northwest wind ($\sim 20\ m\ s^{-1}$) and accumulated in the Aral region (Fig. 4a), leading to the temperature lower than 10 °C at 850 hPa. A strong temperature gradient existed in the southern Uzbekistan and northern Iran due to the cold front (Fig. 4b). The frontal cloud system was captured by MODIS in the Aral Sea region and the dust layer is prominent in the southern Turkmenistan (Fig. 4c). Simultaneously, the northwest wind in northern Iran, Turkmenistan and Uzbekistan increased significantly, which entrained more dust to atmosphere with the dust mass loading reaching up to $5\ g\ m^{-2}$ (Fig. 4d). Compared with the MODIS images, the GOCART, AFWA and Shao04 cases all better demonstrates the evolution of this dust storm which transported eastward from Turkmenistan towards Tajikistan during 13–15 July (see Fig. 5).

4.3. Dust emission

The spatial and temporal evolutions of the dust flux with particle sizes less than 6 μm selected from WRF-Chem using the AFWA dust scheme and their differences from those obtained in GOCART and Shao04 schemes are shown in Fig. 6. Under the strong northwesterly wind speed, dust emission firstly mainly occurred over the east side of Caspian Sea and northern Iran on 12 July, with an emission flux greater than $60\ \mu g\ m^{-2}\ s^{-1}$ in the AFWA case (Fig. 6a). With the eastward

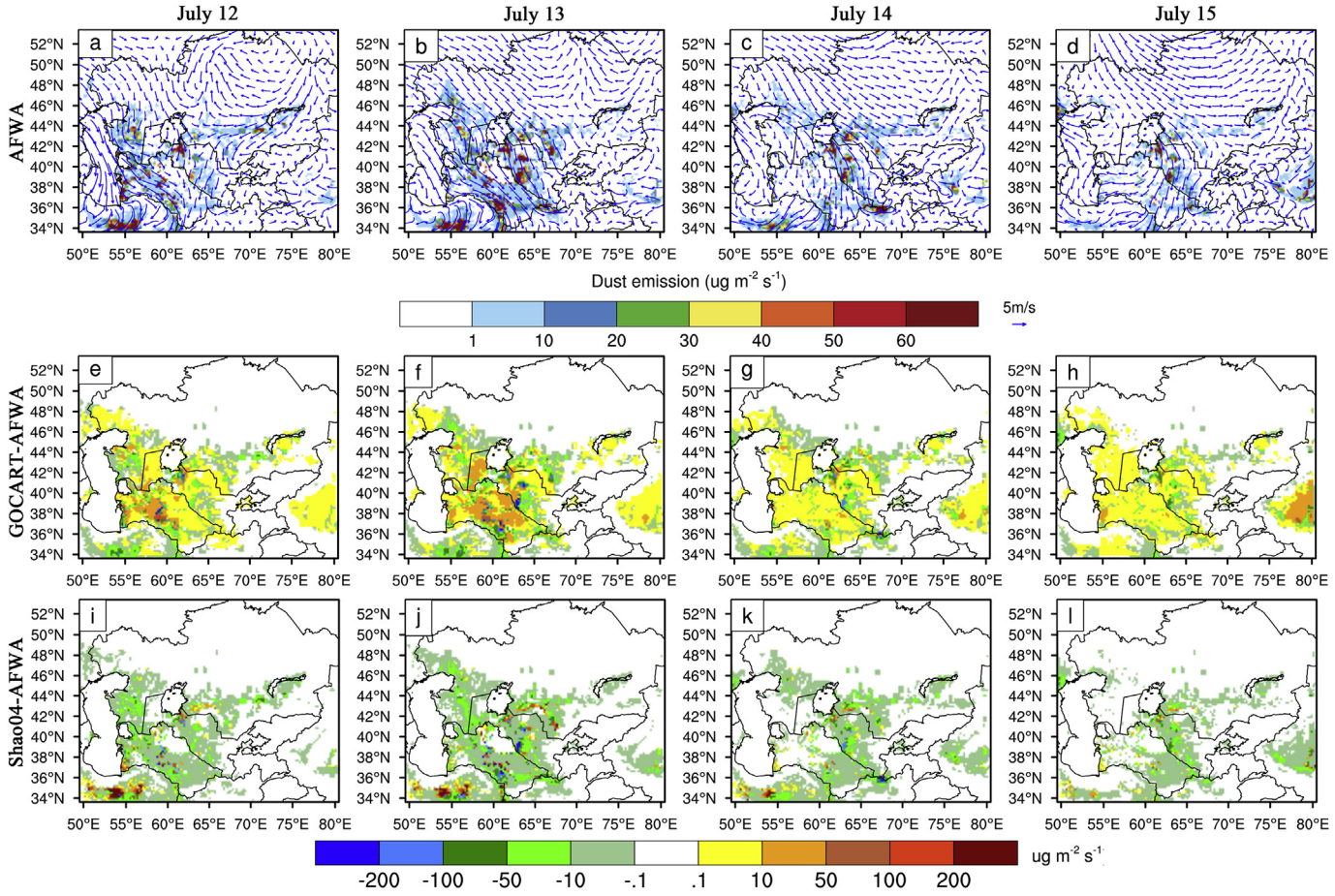

Fig. 6. Spatial distribution of the daily average dust emission flux (particle size less than 6 μm; μm m^{-2} s^{-1}) and wind fields (vectors) in the case of (a–d) AFWA; and the differences of dust emission flux in the cases of (e–h) GOCART and (i–l) Shao04 subtracting that in AFWA during the simulation periods.

Table 2
Daily dust emission (Tg) calculated from GOCART, AFWA and Shao4 dust schemes during the simulation periods.

Time	GOCART		AFWA		Shao04	
	0–10 μm	0–6 μm	0–10 μm	0–6 μm	0–20 μm	0–6 μm
12th July	1.31	0.98	1.38	1.24	4.73	1.86
13th July	1.75	1.31	2.16	1.94	4.81	1.87
14th July	0.81	0.60	1.06	0.95	1.61	0.60
15th July	0.73	0.54	0.63	0.57	0.75	0.26
Total	4.59	3.43	5.23	4.70	11.9	4.59

movement of the cold front on 13 July, the dust emission areas expanded to the Kyzylkum desert and the south of Karakum desert (Fig. 6b). In contrast, the dust emission at the east side of Caspian Sea almost disappeared. The total dust emission at domain reached a peak value of 1.94 Tg (Table 2). After 13 July, the emission areas moved to the region near the south of Uzbekistan by the westerly wind, where the dust flux reached up to 60 μg m^{-2} s^{-1} and the emission flux simultaneously decreased at the Karakum and Kyzylkum deserts due to the weakness of cold air (Fig. 6d). Moreover, the dust storm weakened, and the dust emission at the domain decreased to 0.57 Tg on 15 July, approximately 3–4 times lower than the peak.

The dust flux in GOCART was 0.1–10 μg m^{-2} s^{-1} higher than those in the AFWA and Shao04 cases in most areas, especially at Turkmenistan where the difference could be up to 200 μg m^{-2} s^{-1} on 12 and 13 July (Fig. 6), which can be attributed to the low u_{10t} in GOCART (Fig. 7a). Identical conclusions were also obtained in Wu and Lin (2014) who found that the lower u_{10t} in the GOCART scheme easily led to the release of dust particles, which was not achieved with the emission threshold of the Shao04 scheme. On the contrary, the GOCART case yielded strong underestimation of more than 200 μg m^{-2} s^{-1} in central Uzbekistan and a small part of the Karakum desert on 13 July and 10–100 μg m^{-2} s^{-1} in northern Iran and Uzbekistan during the dust storm. Overall, the GOCART scheme simulated higher dust emission at Turkmenistan and lower dust emission at Uzbekistan and northern Iran compared with the AFWA scheme.

In terms of Shao04 case, large dust flux was concentrated in the regions of northern Iran, small areas of Turkmenistan and the surrounding areas of the southern Aral Sea, where the positive differences were more than 200 μg m^{-2} s^{-1} (Fig. 6i and j). Notably, dust flux in the Shao04 case was 0.1–100 μg m^{-2} s^{-1} lower than that in the AFWA case in most areas of domain which could be attributed to the higher threshold friction velocity (u_{*t}) in the Shao04 case ranging from 0.2 m s^{-1} to 1.5 m s^{-1} (Fig. 7d and g). Therefore, less dust was released in the Shao04 case during the dust storms. For example, as shown in Fig. 7, at 9 UTC on 13 July, although the u_* was the same in both the AFWA and Shao04 schemes, the dust emission in the AFWA case was still larger than that in the Shao04 case in most areas where u_{*t} was lower than that in the Shao04 scheme. In addition, the dust emission area in the GOCART case is the largest, followed by those in the AFWA scheme and Shao04 scheme, due to their differences in u_{*t}. However, Shao04 case produced the largest dust flux in the Karakum desert and Kyzylkum desert, especially when particles reached up to 20 μm, which was consistent with the results of Wu and Lin (2014) and Darmenova et al. (2009). The total dust emission (0–20 μm) of the simulation period in the Shao04 scheme is 11.9 Tg, approximately 2–3 times larger than those in the AFWA and GOCART cases (Table 2). It is important to

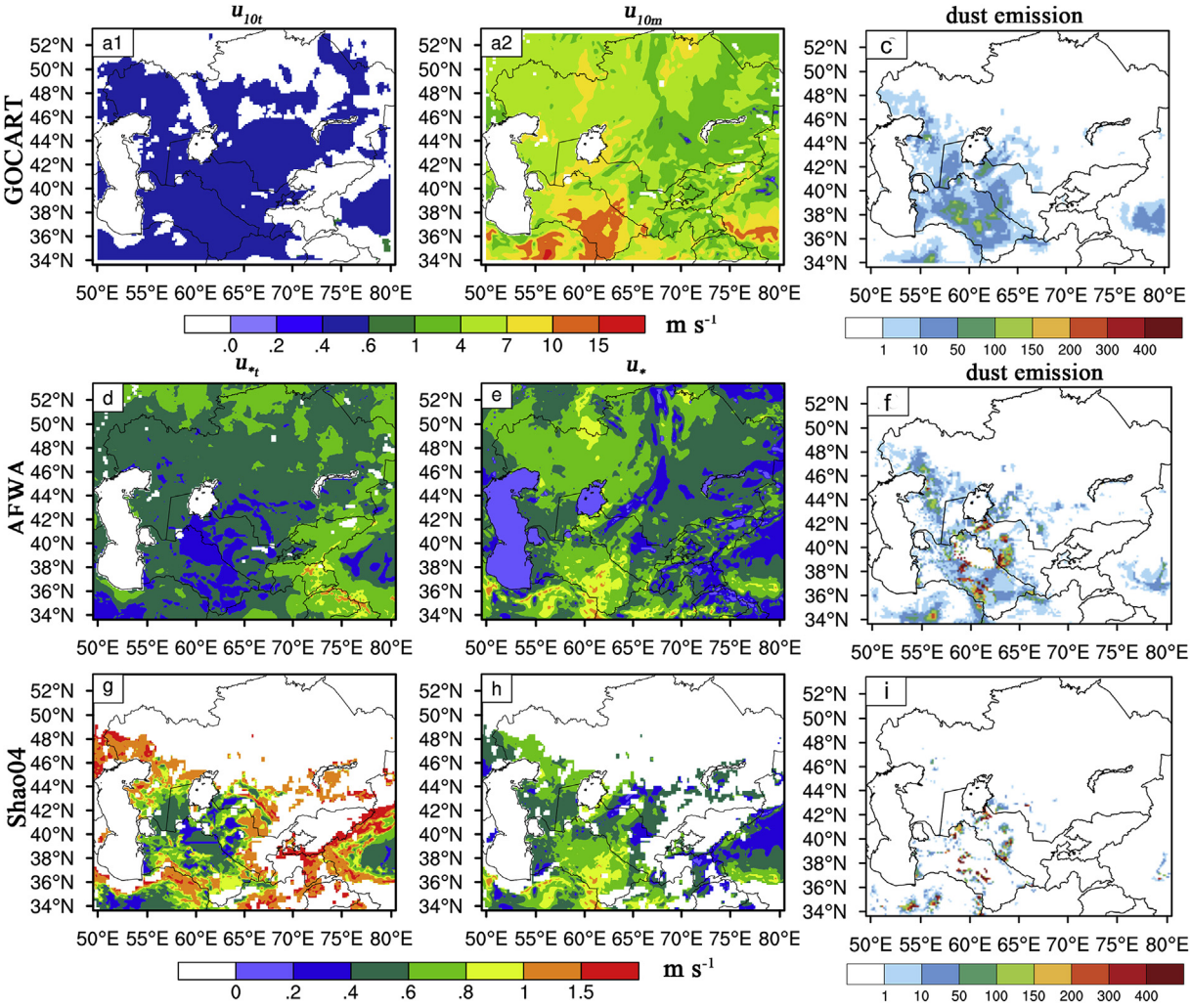

Fig. 7. Spatial distribution of the (a) threshold velocity (u_{10t}), (b) wind speed at 10 m (u_{10m}), and (c) dust emission for the GOCART dust scheme; threshold friction velocity u_{*t}, friction velocity u_* and dust flux (particle sizes less than 6 μm; μm m^{-2} s^{-1}) for (d–f) AFWA and (g–i) Shao04 dust schemes at 09 UTC on July 13.

Table 3
Total dust emission (Tg) in different dust size bins from GOCART, AFWA and Shao4 dust schemes during the simulation periods.

Size bins	GOCART		AFWA		Shao04	
Bin1	0.31	6.7%	0.56	10.7%	0.96	8.1%
Bin2	0.95	20.7%	0.53	10.1%	1.75	14.7%
Bin3	1.05	22.9%	1.09	20.9%	1.89	15.9%
Bin4	1.12	24.4%	2.52	48.2%	3.60	30.3%
Bin5	1.16	25.3%	0.53	10.1%	3.70	31.0%
Total	4.59	100%	5.23	100%	11.90	100%

highlight that the total dust emissions with particle sizes less than 6 μm of the four days in the three dust schemes had slight differences whereas the daily variation was quite different. It can be explained that the GOCART has large dust emission areas but the maximum of emission flux is low while it's opposite to AFWA and Shao04 scheme, leading to similar total dust emission. Yet the spatial and temporal of emission flux in three dust emission shows large difference.

The total dust emission in different size bins is shown in Table 3. The proportions of these emission increases with increasing particle size in the Shao04 and GOCART cases, while the peak value appears (at a value of 48.2%) in the range of 3–6 μm in the AFWA scheme. Moreover, the dust emission with sizes of 6–20 μm in the Shao04 scheme account for more than half of the total dust emission (61.3%). However, the emission with particle sizes of 6–10 μm only account for 25.3% and 10.1% of the total dust emission in the GOCART and AFWA schemes, respectively, due to the fractions in different size classes (Table 1).

4.4. Dust mass loading and transport

To demonstrate the abilities of different dust schemes in the WRF-Chem model to simulate AOD using different schemes, the spatial distributions of the simulated AOD from the GOCART, AFWA and Shao04 dust schemes and the corresponding MODIS observations during the simulation period are shown in Fig. 8. On 12 July, the MODIS AOD was the highest (> 0.5) in the Karakum desert and northern Iran, which were well captured by the Shao04 case. Both the GOCART and AFWA cases only simulated the high AOD in the Karakum desert and underestimated it in northern Iran. The AOD in the AFWA case over northern Iran was 0–0.35, which was higher than that in the GOCART case (0–0.2). The high AOD areas expanded to the Kyzylkum desert on 13 July, which was reproduced by the Shao04 and AFWA cases. The GOCART case significantly underestimated the higher AOD (~0.5) over northern Uzbekistan. After 13 July, the AOD over northern Iran gradually decreased, and the dust storm moved to the south of Uzbekistan, where the AOD increased to 0.5. The AOD in the AFWA case was more consistent with the MODIS AOD, although it was underestimated by ~0.2 over the south of Uzbekistan on 15 July. Moreover, the Shao04 case simulated a higher AOD in the southeastern region of the Aral Sea

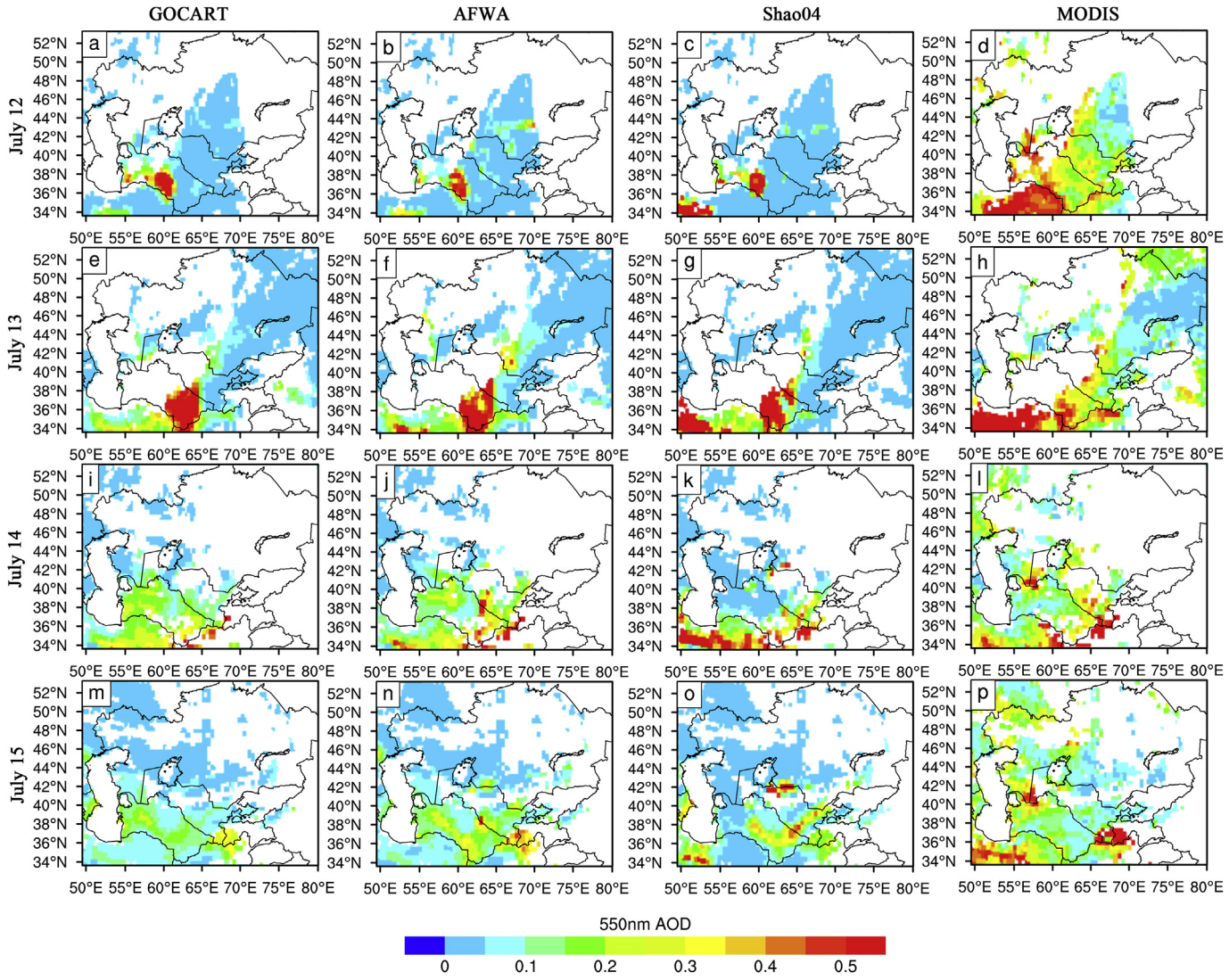

Fig. 8. Spatial distribution of daily average AOD at 550 nm from the WRF-Chem model using (a, e, i and m) GOCART, (b, f, j and n) AFWA and (c, g, k and o) Shao04 dust schemes (all dust size bins), as well as (d, h, l and p) MODIS, during simulation periods.

on 14–15 July compared with the MODIS AOD.

In general, the AOD in the Shao04 and AFWA cases both performed better over Central Asia compared with the MODIS AOD, although the AFWA case only considered dust particle sizes less than 10 μm (Table 2), indicating that small dust particles is more important. The Shao04 case had the best performance when considering northern Iran, except for the overestimation in the southeastern region of the Aral Sea on 14–15 July. The GOCART case only captured the high AOD over Turkmenistan and the south of Uzbekistan and strongly underestimated the AOD at Kyzylkum desert. Both GOCART and AFWA still significantly underestimated the AOD over northern Iran.

The spatial distributions of dust mass loading in three dust schemes were similar to that of the AOD (Fig. 9). The GOCART case mainly simulated high dust mass loading over Turkmenistan, with the value of 1700–3000 mg m^{-2}, which was similar to that of the AFWA case. However, the dust mass loading at northern Iran and the Kyzylkum desert was less than 700 mg m^{-2}, which was approximately 1500 mg m^{-2} lower than that of the AFWA case. Moreover, the dust mass loading in the AFWA and GOCART cases were much lower than that in the Shao04 case over northern Iran, where the erodibility factors were low (Fig. 1). Therefore, the underestimations of AOD over northern Iran in the AFWA and GOCART cases may be mainly attributed to the underestimation of erodibility factors. The AFWA and Shao04 cases simulated the higher dust mass loadings at the Kyzylkum and Karakum deserts, leading to the AOD in the AFWA case closer to the MODIS AOD. Moreover, the Shao04 case simulated high dust mass loading (~2000 mg m^{-2}) in the southeast of the Aral Sea, which corresponded to high AOD. This was mainly due to the effects of the large dust particles considered by the Shao04 case, i.e., because the dust mass loading in the Shao04 case is similar to that in the AFWA case when the dust particle size was less than 6 μm. (Fig. A1). The large divergence of AOD over the south of the Aral Sea in the Shao04 case may be associated with the soil particle size distribution dataset, which could lead to large uncertainties in dust emission (Shao et al., 2011b).

4.5. Vertical structure of dust storm

The AOD was the highest (~1.8) at 36°N–38°N, where the dust and polluted dust extinction reached up to 0.5 km^{-1} (Fig. 10b and c). Compared with the CALIPSO observations, the extinction coefficients in the GOCART, AFWA and Shao04 cases are generally consistent with the observation. Moreover, the dust extinction coefficient at 4–6 km reached up to ~0.28 km^{-1} in the Shao04 case, which was the closest to the CALIPSO observation. Both the AFWA and GOCART cases simulated large extinction coefficients below 2.5 km (0.28–0.5 km^{-1}) at 36°N–42°N but significantly underestimated the extinction coefficients

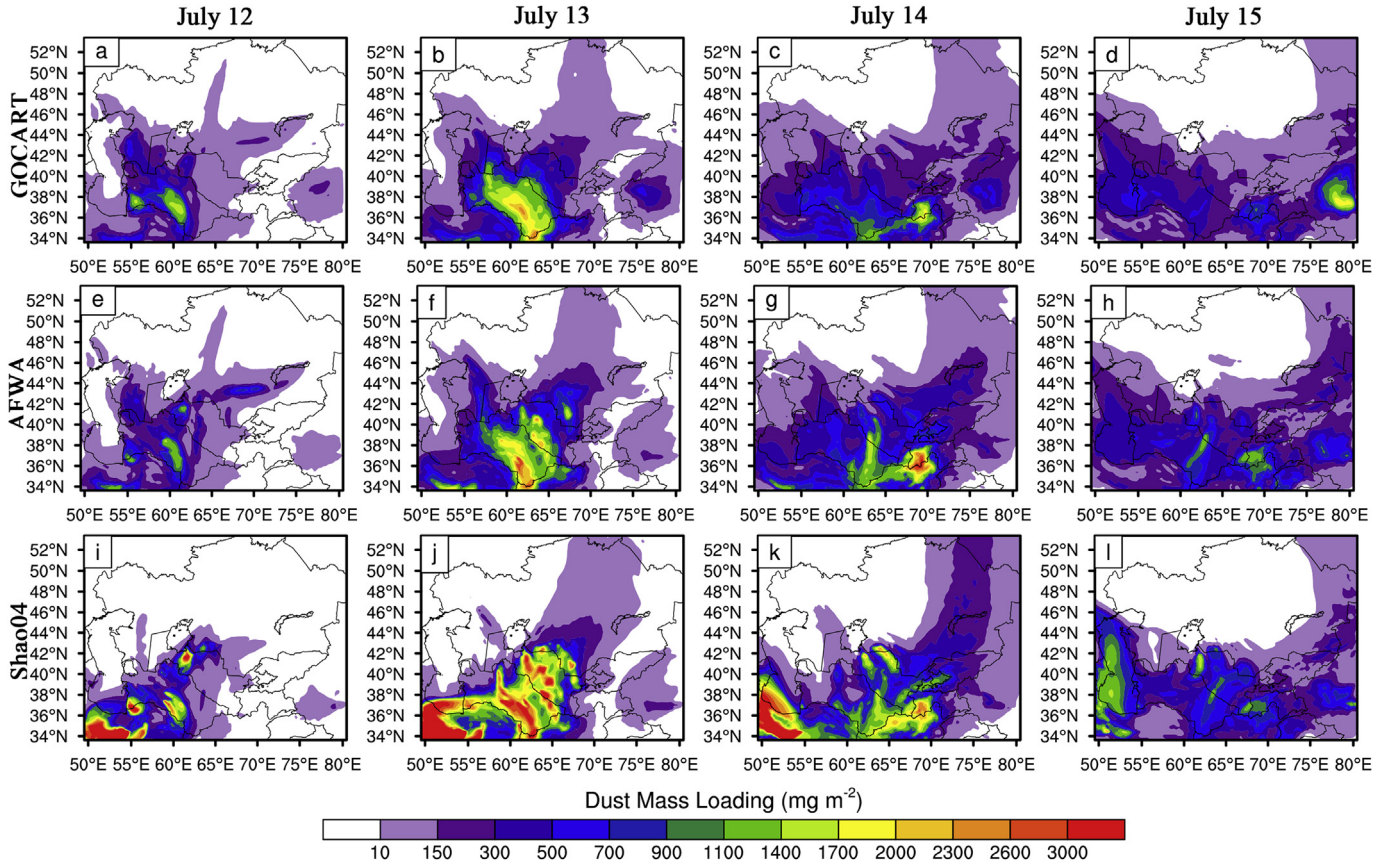

Fig. 9. Spatial distribution of daily average dust loading (all dust size bins; mg m^{-2}) simulated from the WRF-Chem model using (a–d) GOCART, (e–h) AFWA and (i–l) Shao04 dust schemes during simulation periods.

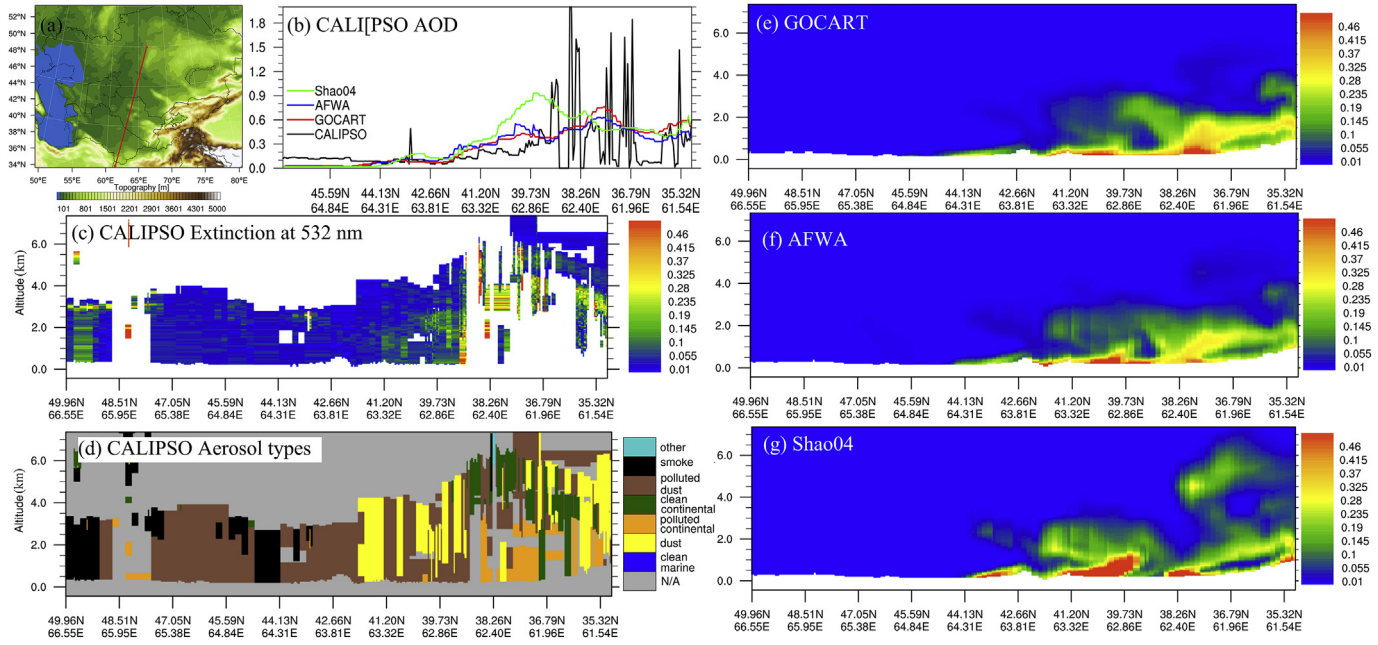

Fig. 10. Vertical profiles of CALIPSO-retrieved (b) AOD, (c) aerosol extinction coefficients and (d) aerosol types and corresponding extinction coefficients simulated by the WRF-Chem model using (e) GOCART, (f) AFWA, and (g) Shao04 dust schemes (all dust size bins) at 21 UTC on 13 July 2016.

above 2.5 km. The peak values of AOD in AFWA and GOCART were 0.6–0.9 at 37°N, which were similar to the CALIPSO AOD (Fig. 10b). In addition, the larger extinction coefficient and AOD in the Shao04 scheme at 39–41 °N was mainly influenced by the large dust particle emission because the dust concentration in Fig. 11 was similar to that in the AFWA case when the dust particle size was less than 6 μm (Fig. A2). Chen et al. (2014) also pointed that the vertical structure of aerosol in WRF-Chem model using GOCART scheme showed large divergence compared with that from micro-pulse lidar and it may be improved by assimilating the dust extinction from micro-pulse lidar.

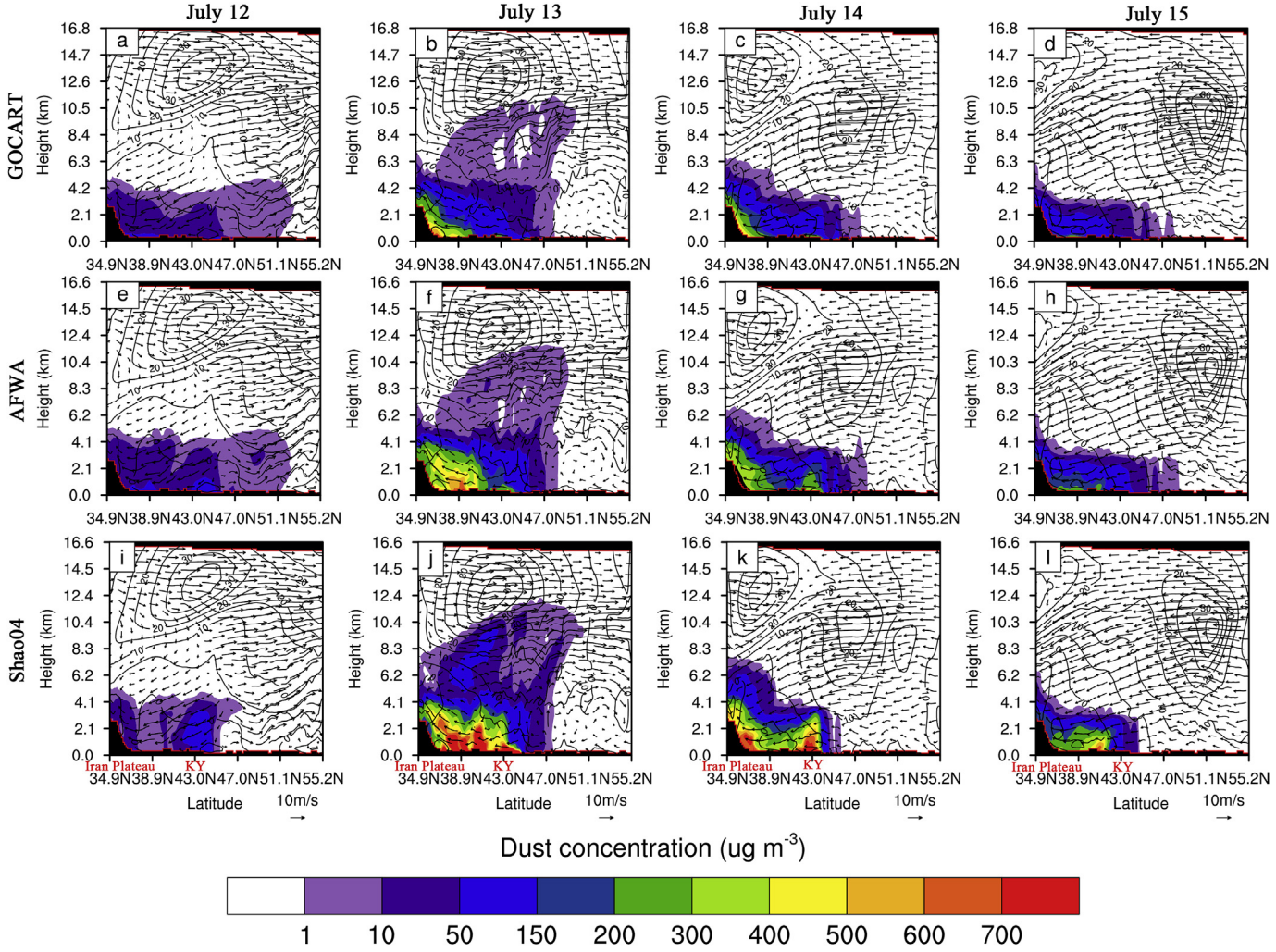

Fig. 11. Cross section of dust concentration (all dust size bins; color scale; ug m^{-3}), zonal wind (contour lines; m s^{-1}) and meridional circulation (vectors) along 65°E from the WRF-Chem simulations using the GOCART (a–d), AFWA (e–h) and Shao04 (i–l) schemes during simulation periods. (For interpretation of the references to color in this figure legend, the reader is referred to the Web version of this article.)

Fig. 11 shows the cross section of dust concentration, zonal wind and meridional circulation along 65°E. The cold front moved to Turkmenistan and Uzbekistan on 13 July (Fig. 4). Simultaneously, the wind speed increased to 9.5 m s^{-1} and the pressure increased considerably, but the maximum temperature decreased to ~36 °C (Fig. 3). Under the strong cold front, the dust particles were uplifted to 10 km, accompanied by vertical motion through frontal lifting (Fig. 11b, f and 11j). Considering the total dust bins, the dust concentrations in the GOCART and AFWA cases were 400–600 μg m^{-3} near the surface and 1–10 μg m^{-3} at 5–10 km. In contrast, the dust concentrations in the Shao04 case were much higher, with maximum values of more than 700 μg m^{-3} below 3 km and 1–150 μg m^{-3} from 3 to 10 km, which were similar to the patterns of the extinction coefficient (Fig. 10g). It must also be mentioned that the dust particles were transported southward to the Iran Plateau by north wind near the surface and transported northward by south wind at 4–10 km, which was mainly influenced by the cold front. After 13 July, the strong westerly wind in the high atmosphere dipped down to 4–10 km, and the south wind turned into north wind. Simultaneously, the dust particles in the high atmosphere were transported eastward and southward, leading to the lowest dust concentrations. Moreover, the dust concentrations in the Shao04 case were much larger than those in the GOCART and AFWA cases due to the large dust particle size.

5. Conclusion and discussions

The abilities of the GOCART, AFWA and Shao04 dust schemes coupled to the WRF-Chem model to simulate dust storms were examined in this study by simulating a severe dust storm that occurred in Central Asia from 12 to 15 July 2016. In general, the dust storm was caused by a vortex at 500 hPa and cold front. Both the spatial and temporal variations of the meteorological field were reproduced well by the WRF-Chem model compared with in situ measurements. Comparisons with satellite retrievals revealed that the Shao04 case reproduced the spatial and temporal variation of dust storms well in northern Iran, Turkmenistan and part of Uzbekistan. The AFWA simulated AOD as better as the Shao04 case except for northern Iran. It should be pointed that the Shao04 scheme uses large size range (0–20 μm) and the AFWA scheme only uses small sizes range (0–10 μm), indicating smaller size particles may have significant radiation effects and can be entrained to a higher vertical level compared with large size particles. The GOCART scheme showed a good agreement with MODIS AOD at Karakum desert, but significantly underestimated the dust emission at the Kyzylkum desert. Both the AFWA and GOCART cases simulated lower AOD over northern Iran but the AOD in AFWA case was better than that in the GOCART case. The dust emission areas in the GOCART scheme were larger than those in the AFWA and Shao04 schemes. However, the maximum of dust flux at dust source region in

GOCART was much lower than that in AFWA and Shao04 scheme. Therefore, the four-day total dust emissions in the model domain of three dust schemes were similar with particles less than 6 μm (Table 2). Nevertheless, the total dust emission of all bins in the Shao04 scheme (11.9 Tg) was 2–3 times larger than those in the AFWA (5.23 Tg) and GOCART (4.59 Tg) schemes because large dust particle size range were considered in the Shao04 scheme.

The erodibility, u_{*t}/u_{10t}, particle size distributions are the key parameters used to determine dust flux. Both AFWA and GOCART use the erodibility to calculate the dust flux. Therefore, the reliability of erodibility affects the accuracy of dust flux calculation to some extent. The underestimation of the AOD in the GOCART and AFWA cases over northern Iran may owe to the large uncertainties of the erodibility dataset which is expected to be improved by using normalized difference vegetation index obtained from satellites (Kim et al., 2013). The u_{10t} in the GOCART scheme, u_{*t} in the AFWA and Shao04 scheme were also compared. Generally, the Shao04 scheme has the highest u_{*t} and GOCART has lower u_{10t}, which leading to less dust released in most areas during the four days in Shao04 scheme. But the variations of dust flux in Sha04 scheme were more sensitive to the cold front. Hence, the total dust emissions had slight differences but the daily variations of the dust emission in three dust schemes were different when the particle size is less than 6 μm. Xi and Sokolik (2016a) also found that the large differences of dust emission in different schemes may be due to the different sensitivities of u_{*t} to the surface roughness. The improvements of the emitted particle size distribution, saltation algorithm and u_{*t} in the AFWA scheme are responsible for its better performance compared with that of the GOCART scheme (Jones et al., 2012). Besides, Shao04 scheme uses the $p_f(d)$ and $p_m(d)$ of parent soil to calculate the size distribution of dust particles. Since the parent soil particle size dataset is a major factor that influences the performance of Shao04 scheme (Shao et al., 2011b), the higher AOD to the southeast of the Aral Sea in Shao04 scheme may be associated with the uncertainties in the parent soil particle size distribution dataset. Thus, accurate measurements of erodibility datasets and soil particle size distributions are urgently needed in the future.

Overall, the Shao04 and AFWA dust schemes can be used to simulate or forecast dust storms over Central Asia. However, due to lack of ground-based aerosol observations, there are still some uncertainties in evaluating the model performance. Besides, this study only considered natural desert dust. The degradation of the Aral Sea has been recognized as the most serious ecological disaster since the 1960s and formed the present Aralkum desert due to the expansion of agricultural irrigation and the increase in population (Dukhovny, 2008; Saiko and Zonn, 2000; Indoitu et al., 2015). It indicated that the dust emission from agriculture and Aralkum accounted for 18.3–56.5% of total dust emission (Xi and Sokolik, 2016b). In the future, we will develop an anthropogenic dust emission scheme and couple it to the WRF-Chem model to improve the ability of the WRF-Chem model to forecast dust storms over Central Asia.

Declaration of interests

The authors declare that they have no known competing financial interests or personal relationships that could have appeared to influence the work reported in this paper.

Acknowledgments

This research was supported by the Foundation for National Natural Science Foundation of China (No. 91837103, 41775003); Innovative Research Groups of the National Science Foundation of China (Grant No. 41521004); and the China 111 Project (No. B13045) and Foundation of Key Laboratory for Semi-Arid Climate Change of the Ministry of Education in Lanzhou University (No. lzujbky-2017-kb02).

Appendix A. Supplementary data

Supplementary data to this article can be found online at https://doi.org/10.1016/j.atmosenv.2019.03.014.

References

Abuduwaili, J., Liu, D.W., Wu, G.Y., 2010. Saline dust storms and their ecological impacts in arid regions. J. Arid Land. 2 (2), 144–150. https://doi.org/10.3724/SP.J.1227.2010.00144.

Chen, B., Huang, J.P., Minnis, P., Hu, Y., Yi, Y., Liu, Z., Zhang, D., Wang, X., 2010. Detection of dust aerosol by combining CALIPSO active lidar and passive IIR measurements. Atmos. Chem. Phys. 10, 4241–4251. https://doi.org/10.5194/acp-10-4241-2010.

Chen, F., Dudhia, J., 2001. Coupling an advanced land surface–hydrology model with the penn state–NCAR MM5 modeling system, Part I: model implementation and sensitivity. Mon. Weather Rev. 129, 569–585. https://doi.org/10.1175/1520-0493(2001)129<0587:CAALSH>2.0.CO;2.

Chen, F., Mitchell, K., Schaake, J., Xue, Y.K., Pan, H.-L., Koren, V., Duan, Q.Y., Ek, M., Betts, A., 1996. Modeling of land surface evaporation by four schemes and comparison with FIFE observations. J. Geophys. Res. Atmos. 101, 7251–7268. https://doi.org/10.1029/95JD02165.

Chen, S.Y., Huang, J.P., Kang, L.T., Wang, H., Ma, X.J., He, Y.L., Yuan, T.G., Yang, B., Huang, Z.W., 2017b. Emission, transport and radiative effects of mineral dust from Taklimakan and Gobi Deserts Comparison of measurements and model results. Atmos. Chem. Phys. 17, 1–43. https://doi.org/10.5194/acp-17-2401-2017.

Chen, S.Y., Huang, J.P., Qian, Y., Zhao, C., Kang, L.T., Yang, B., Liu, Y.Z., Yuan, T.G., Wang, T.H., Ma, X.J., Zhang, G.L., 2017a. An overview of mineral dust modeling over East Asia. J. Meteor. Res. 31, 633–653. https://doi.org/10.1007/s13351-017-6142-2.

Chen, S.Y., Huang, J.P., Zhao, C., Qian, Y., Leung, L.R., Yang, B., 2013. Modeling the transport and radiative forcing of Taklimakan dust over the Tibetan Plateau: a case study in the summer of 2006. J. Geophys. Res. Atmos. 118, 797–812. https://doi.org/10.1002/jgrd.50122.

Chen, S.Y., Yuan, T.G., Zhang, X.R., Zhang, G.L., Feng, T.C., Zhao, D., Zang, Z., Liao, S.J., Ma, X.J., Jiang, N.X., Zhang, J., Yang, F., Lu, H., 2018. Dust modeling over East Asia during the summer of 2010 using the WRF-Chem model. J. Quant. Spectrosc. Radiat. Transf. 213, 1–12. https://doi.org/10.1016/j.jqsrt.2018.04.013.

Chen, S.Y., Zhao, C., Qian, Y., Leung, L.R., Huang, J.P., Huang, Z.W., Bi, J.R., Zhang, W., Shi, J.S., Yang, L., Li, D., Li, J.X., 2014. Regional modeling of dust mass balance and radiative forcing over East Asia using WRF-Chem. Aeolian. Res. 15, 15–30. https://doi.org/10.1016/j.aeolia.2014.02.001.

Chin, M., Rood, R.B., Lin, S.-J., Müller, J.-F., Thompson, A.M., 2000. Atmospheric sulfur cycle simulated in the global model GOCART: model description and global properties. J. Geophys. Res. Atmos. 105 (D20), 24671–24688. https://doi.org/10.1029/2000JD900384.

Darmenova, K., Sokolik, I., Shao, Y.P., Marticorena, B., Bergametti, G., 2009. Development of a physically based dust emission module within the Weather Research and Forecasting (WRF) model: assessment of dust emission parameterizations and input parameters for source regions in Central and East Asia. J. Geophys. Res. 114, D14. https://doi.org/10.1029/2008JD011236.

Dukhovny, V.A. (Ed.), 2008. Comprehensive Remote Sensing and Ground Based Studies of the Dried Aral Sea Bed, SIC ICWC. Tashkent, pp. 173.

Fast, J.D., Gustafson, W.I., Easter, R.C., Zaveri, R.A., Barnard, J.C., Chapman, E.G., Grell, G.A., Peckham, S., 2006. Evolution of ozone, particulates, and aerosol direct radiative forcing in the vicinity of Houston using a fully coupled Meteorology-Chemistry-Aerosol Model. J. Geophys. Res. 111, D21305. https://doi.org/10.1029/2005JD006721.

Gillette, D., 1979. Environmental factors affecting dust emission by wind erosion. In: Saharan Dust. Wiley, New York, pp. 71–94.

Ginoux, P., Chin, M., Tegen, I., Prospero, J.M., Holben, B., Dubovik, O., Lin, S.-J., 2001. Sources and distributions of dust aerosols simulated with the GOCART model. J. Geophys. Res. 106, 20255–20273. https://doi.org/10.1029/2000JD000053.

Grell, G.A., Peckham, S.E., Schmitz, R., McKeen, S.A., Frost, G., Skamarock, W.C., Eder, B., 2005. Fully coupled "online" chemistry within the WRF model. Atmos. Environ. 39, 6957–6975. https://doi.org/10.1016/j.atmosenv.2005.04.027.

Groll, M., Opp, C., Aslanov, I., 2013. Spatial and temporal distribution of the dust deposition in Central Asia – results from a long term monitoring program. Aeolian. Res. 9, 49–62. https://doi.org/10.1016/j.aeolia.2012.08.002.

Guo, J., Yin, Y., 2015. Mineral dust impacts on regional precipitation and summer circulation in East Asia using a regional coupled climate system model. J. Geophys. Res. Atmos. 120, 10378–10398. https://doi.org/10.1002/2015JD023096.

Han, Z.W., Li, J.W., Xia, X.G., Zhang, R.J., 2012. Investigation of direct radiative effects of aerosols in dust storm season over East Asia with an online coupled regional climate-chemistry-aerosol model. Atmos. Environ. 54 (4), 688–699. https://doi.org/10.1016/j.atmosenv.2012.01.041.

Hanna, S., Yang, R., Yin, X.T., 2000. Evaluations of numerical weather prediction (NWP) models from the point of view of in-puts required by atmospheric dispersion models. Int. J. Environ. Pollut. 14, 98–105. https://doi.org/10.1504/IJEP.2000.000530.

Hofer, J.L., Althausen, D., Abduvosit, S.F., Makhmudov, A.N., Nazarov, B.I., Schettler, G., Engelmann, R., Baars, H., Fomba, K.W., Mueller, K., Heinold, B., Kandler, K., Ansmann, A., 2017. Long-term profiling of mineral dust and pollution aerosol with multiwavelength polarization/Raman lidar at the Central Asian site of Dushanbe, Tajikistan: case studies. Atmos. Chem. Phys. 17, 14559–14577. https://doi.org/10.5194/acp-17-14559-2017.

Hong, S.-Y., Noh, Y., Dudhia, J., 2006. A new vertical diffusion package with an explicit treatment of entrainment processes. Mon. Weather Rev. 134, 2318–2341. https://doi.org/10.1175/MWR3199.1.
Hsu, N.C., Jeong, M.-J., Bettenhausen, C., Sayer, A.M., Hansell, R., Seftor, C., Huang, J.B., Tsay, S.C., 2013. Enhanced Deep Blue aerosol retrieval algorithm: the second generation. J. Geophys. Res. Atmos. 118, 9296–9315. https://doi.org/10.1002/jgrd.50712.
Hsu, N.C., Tsay, S.C., King, M.D., Herman, J., 2006. Deep blue retrievals of asian aerosol properties during ACE-asia. IEEE Trans. Geosci. Remote Sens. 44, 3180–3195. https://doi.org/10.1109/TGRS.2006.879540.
Huang, J.P., Li, Y., Fu, C.B., Chen, F.H., Fu, Q., Dai, A., Shinoda, M., Ma, Z.G., Guo, W.,D., Li, Z.Q., Zhang, L., Liu, Y., Yu, H.P., He, Y.L., Xie, Y., Guan, X.D., Ji, M., Lin, L., Wang, S.S., Yan, H.R., Wang, G.Y., 2017. Dryland climate change: recent progress and challenges. Rev. Geophys. 55, 719–778. https://doi.org/10.1002/2016RG000550.
Huang, J.P., Ge, J.M., Weng, F.Z., 2007. Detection of Asia dust storms using multisensor satellite measurements. Remote Sens. Environ. 110, 186–191. https://doi.org/10.1016/j.rse.2007.02.022.
Huang, J.P., Ji, M.X., Xie, Y.K., Wang, S.S., He, Y.L., Ran, J.J., 2015a. Global semi-arid climate change over last 60 years. Clim. Dyn. 46, 1131–1150. https://doi.org/10.1007/s00382-015-2636-8.
Huang, J.P., Liu, J.J., Chen, B., Nasiri, S.L., 2015b. Detection of anthropogenic dust using CALIPSO lidar measurements. Atmos. Chem. Phys. 15 (7), 10163–10198. https://doi.org/10.5194/acp-15-11653-2015.
Huang, J.P., Wang, T.H., Wang, W.C., Li, Z.Q., Yan, H.R., 2014. Climate effects of dust aerosols over East Asian arid and semiarid regions. J. Geophys. Res. Atmos. 119, 11398–11416. https://doi.org/10.1002/2014JD021796.
Huang, J.P., Yu, H.P., Guan, X.D., Wang, G.Y., Guo, R.X., 2016. Accelerated dryland expansion under climate change. Nat. Clim. Change 6, 166–171. https://doi.org/10.1038/NCLIMATE2837.
Huneeus, N., Schulz, M., Balkanski, Y., Griesfeller, J., Prospero, J.M., Kinne, S., Bauer, S., Boucher, O., Chin, M., Dentener, F., Diehl, T., Easter, R.C., Fillmore, D., Ghan, S.J., Ginoux, P., Grini, A., Horowitz, L.W., Koch, D., Krol, M., Landing, W.M., Liu, X.H., Mahowald, N., Miller, R., Morcrette, J.-J., Myhre, G., Penner, J.E., Perlwitz, J.P., Stier, P., Takemura, T., Zender, C.S., 2011. Global dust model intercomparison in AeroCom phase I. Atmos. Chem. Phys. 11, 7781–7816. https://doi.org/10.5194/acp-11-7781-2011.
Iacono, M., Mlawer, E., Clough, S., Morcrette, J., 2000. Impact of an improved longwave radiation model, RRTM. on the energy budget and thermodynamic properties of the NCAR community climate mode, CCM3. J. Geophys. Res. 105, 14873–14890. https://doi.org/10.1029/2000JD900091.
Indoitu, R., Kozhoridze, G., Batyrbaeva, M., Vitkovskaya, I., Orlovsky, N., Blumberg, D., Orlovsky, L., 2015. Dust emission and environmental changes in the dried bottom of the Aral Sea. Aeolian. Res. 17, 101–115. https://doi.org/10.1016/j.aeolia.2015.02.004.
Indoitu, R., Orlovsky, L., Orlovsky, N., 2012. Dust storms in central Asia: spatial and temporal variations. J. Arid Environ. 85, 62–70. https://doi.org/10.1016/j.jaridenv.2012.03.018.
Jimenez, P.A., Dudhia, J., Gonzalez-Rouco, J.F., Navarro, J., Montavez, J.P., Garcia-Bustanmante, E., 2012. A revised scheme for the WRF surface layer formulation. Mon. Weather Rev. 140 (3), 898–918. https://doi.org/10.1175/MWR-D-11-00056.1.
Jones, S.L., Adams-Selin, R., Hunt, E.D., Creighton, G.A., Cetola, J.D., 2012. Update on Modifications to WRF-CHEM GOCART for Fine-Scale Dust Forecasting at AFWA. American Geophysical Union Fall Meeting Abstracts.
Jones, S.L., Creighton, G.A., Kuchera, E.L., Rentschler, S.A., 2010. Adapting WRF-CHEM GOCART for Fine-Scale Dust Forecasting. American Geophysical Union Fall Meeting Abstracts.
Kain, J., Fritsch, J., 1990. A one-dimensional entraining/detraining plume model and its application in convective parameterization. J. Atmos. Sci. 47 (23), 2784–2802. https://doi.org/10.1175/1520-0469(1990)047<2784:AODEPM>2.0.CO;2.
Kain, J.S., 2004. The kain–fritsch convective parameterization: an update. J. Appl. Meteorol. Clim. 43, 170–181. https://doi.org/10.1175/15200450(2004)043<0170:TKCPAU>2.0.CO;2.
Kameda, T., Azumi, E., Fukushima, A., Tang, N., Matsuki, A., Kamiya, Y., Toriba, A., Hayakawa, K., 2016. Mineral dust aerosols promote the formation of toxic nitropolycyclic aromatic compounds. Sci. Rep. 6, 24427. https://doi.org/10.1038/srep24427.
Kim, D., Chin, M., Bian, H.S., Tan, Q., Brown, M.E., Zheng, T., You, R.J., Diehl, T., Ginoux, P., Kucsera, T.L., 2013. The effect of the dynamic surface bareness on dust source function, emission, and distribution. J. Geophys. Res. Atmos. 118, 871–886. https://doi.org/10.1029/2012JD017907.
Kok, J.F., 2011. A scaling theory for the size distribution of emitted dust aerosols suggests climate models underestimate the size of the global dust cycle. Proc. Natl. Acad. Sci. U.S.A. 108 (3), 1016–1021. https://doi.org/10.1073/pnas.1014798108.
Marticorena, B., Bergametti, G., 1995. Modeling the atmospheric dust cycle: 1. Design of a soil-derived dust emission scheme. J. Geophys. Res. 100 (D8), 16415–16430. https://doi.org/10.1029/95JD00690.
Middleton, N.J., 2017. Desert dust hazards: a global review. Aeolian. Res. 24, 53–63. https://doi.org/10.1016/j.aeolia.2016.12.001.
Mlawer, E., Taubman, S., Brown, P., Iacono, M., Clough, S., 1997. Radiative transfer for inhomogeneous atmospheres: RRTM, a validated correlated-k model for the longwave. J. Geophys. Res. 102, 16663–16682. https://doi.org/10.1029/97JD00237.
Morrison, H., Curry, J.A., Khvorostyanov, V.I., 2005. A new double moment microphysics parameterization for application in cloud and climate models. Part I: Description. J. Atmos. Sci. 62, 1665–1677. https://doi.org/10.1175/JAS3446.1.
Ochmann, U., Nowak, D., 2009. Inhalationsbedingte chemische Lungenschadigung. Pneumologe. Pneumologe. 6 (1), 22–29. https://doi.org/10.1007/s10405-008-0229-5.
Opp, C., 2005. Desertification in Uzbekistan. Geographische Rundschau International Edition 1 (2), 12–20.
Opp, C., Groll, M., Aslanov, I., Lotz, T., Vereshagina, N., 2017. Aeolian dust deposition in the southern Aral Sea region (Uzbekistan): ground-based monitoring results from the LUCA project. Quat. Int. 429, 86–99. https://doi.org/10.1016/j.quaint.2015.12.103.
Orlovsky, L., Orlovsky, N., Durdyevb, A., 2005. Dust storms in Turkmenistan. J. Arid Environ. 60, 83–97. https://doi.org/10.1016/j.jaridenv.2004.02.008.
Orlovsky, L., Tolkacheva, G., Orlovsky, N., Mamedov, B., 2004. Dust storms as a factor of atmospheric air pollution in the Aral Sea basin. Air. Pollut. 12, 353–362. https://doi.org/10.2495/AIR040351.
Popov, V.A., 1998. The role of salt migration in the landscape genesis of the Priaral region. Probl. Desert Dev. 3–4, 122–126.
Prospero, J., 1999. Long-term measurements of the transport of African mineral dust to the southeastern United States: implications for regional air quality. J. Geophys. Res. Atmos. 104, 15917–15928. https://doi.org/10.1029/1999JD900072.
Rashki, A., Kaskaoutisb, D.G., Sepehr, A., 2018. Statistical evaluation of the dust events at selected stations in southwest Asia: from the Caspian Sea to the arabian sea. Catena 165, 590–603. https://doi.org/10.1016/j.catena.2018.03.011.
Saiko, T.A., Zonn, I.S., 2000. Irrigation expansion and dynamics of desertification in the Circum-Aral region of Central Asia. Appl. Geogr. 20, 349–367. https://doi.org/10.1016/S0143-6228(00)00014-X.
Shao, Y., 2004. Simplification of a dust emission scheme and comparison with data. J. Geophys. Res. 109, D10202. https://doi.org/10.1029/2003JD004372.
Shao, Y., Ishizuka, M., Mikami, M., Leys, J.F., 2011b. Parameterization of size-resolved dust emission and validation with measurements. J. Geophys. Res. 116, D08203. https://doi.org/10.1029/2010JD014527.
Shao, Y.P., Wyrwoll, K.-H., Chappell, A., Huang, J.P., Lin, Z.H., McTainsh, G.H., Mikami, M., Tanaka, T.Y., Wang, X.L., Yoon, S., 2011a. Dust cycle: an emerging core theme in Earth system science. Aeolian. Res. 2, 181–204. https://doi.org/10.1016/j.aeolia.2011.02.001.
Sternberg, T., Edwards, M., 2017. Desert dust and health: a central asian review and steppe case study. Int. J. Environ. Res. Public Health 14, 1342. https://doi.org/10.3390/ijerph14111342.
Su, L., Fung, J.C.H., 2015. Sensitivities of WRF-Chem to dust emission schemes and land surface properties in simulating dust cycles during springtime over East Asia. J. Geophys. Res. Atmos. 120, 11215–11230. https://doi.org/10.1002/2015JD023446.
Tanaka, T.Y., Chiba, M., 2006. A numerical study of the contributions of dust source regions to the global dust budget. Glob. Planet. Chang. 52, 88–104. https://doi.org/10.1016/j.gloplacha.2006.02.002.
Textor, C., Schulz, M., Guibert, S., Kinne, S., Balkanski, Y., Bauer, S., Berntsen, T., Berglen, T.F., Boucher, O., Chin, M., Dentener, F., Diehl, T., Easter, R.C., Feichter, H., Fillmore, D., Ghan, S.J., Ginoux, P., Gong, S.P., Grini, A., Hendricks, J., Horowitz, L.W., Huang, P., Isaksen, I., Iversen, T., Kloster, S., Koch, D., Kirkevag, A., Kristjansson, J.E., Krol, M., Lauer, A., Lamarque, J.F., Liu, X., Montanaro, V., Myhre, G., Penner, J., Pitari, G., Lamarque, J.F., Liu, X., Montanaro, V., Myhre, G., Penner, J., Pitari, G., Reddy, E.S.P., Seland, Ø., Stier, P., Takemura, T., Tie, X., 2006. Analysis and quantification of the diversities of aerosol life cycles within AeroCom. Atmos. Chem. Phys. 6, 1777–1813. https://doi.org/10.5194/acp-6-1777-2006.
Usmanov, V.O., 1998. Estimation of the influence of dusty salt transfer on the productivity of agricultural crops in the Priaral region. Probl. Desert Dev. 3–4, 147–151.
Vaughan, M.A., Young, S.A., Winker, D.M., Powell, K.A., Omar, A.H., Liu, Z.Y., Hu, Y.X., Hostetler, C.A., 2004. Fully automated analysis of space-based lidar data: an overview of the CALIPSO retrieval algorithms and data products. Proc. SPIE 5575, 16–30. https://doi.org/10.1117/12.572024.
Wang, F., Zhao, X.Q., Gerlein-Safdi, C., Mu, Y., Wang, D.F., Lu, Q., 2017. Global sources, emissions, transport and deposition of dust and sand and their effects on the climate and environment: a review. Front. Environ. Sci. Eng. 11 (1), 13. https://doi.org/10.1007/s11783-017-0904-z.
Wang, S.-H., Hsu, N.C., Tsay, S.-C., Lin, N.-H., Sayer, A.M., Huang, S.-J., Lau, W.K.M., 2012. Can Asian dust trigger phytoplankton blooms in the oligotrophic northern South China Sea. Geophys. Res. Lett. 39, L05811. https://doi.org/10.1029/2011GL050415.
Winker, D.M., Pelon, J., McCormick, M.P., 2003. The CALIPSO mission: spaceborne lidar for observation of aerosols and clouds. Proc. SPIE 4893, 1–11. https://doi.org/10.1117/12.466539.
Wu, C.L., Lin, Z.H., 2014. Impact of two different dust emission schemes on the simulation of a severe dust storm in East Asia using the WRF-Chem model. Clim. Environ. Res. (in Chinese) 19 (4), 419–436. https://doi.org/10.3878/j.issn.1006-9585.2013.13041.
Wu, J., Fu, C.B., Han, Z.W., Tang, J.P., Xu, Y.Y., Zhang, R.J., 2013. Simulation of the direct effects of dust aerosol on climate in East Asia. Particuology 8, 301–307. https://doi.org/10.1016/j.partic.2010.01.006.
Xi, X., Sokolik, I.N., 2016a. Dust interannual variability and trend in Central Asia from 2000 to 2014 and their climatic linkages. J. Geophys. Res. Atmos. 120, 12175–12197. https://doi.org/10.1002/2015JD024092.
Xi, X., Sokolik, I.N., 2016b. Quantifying the anthropogenic dust emission from agricultural land use and desiccation of the Aral Sea in Central Asia. J. Geophys. Res. Atmos. 121, 1–12. https://doi.org/10.1002/2016JD025556.
Yang, B., Qian, Yun, Berg, L.K., Ma, P.-L., Wharton, S., Bulaevskaya, V., Yan, H.P., Zhang, S.H., Shaw, W.J., 2017. Sensitivity of turbine-height wind speeds to parameters in planetary boundary-layer and surface-layer schemes in the weather research and forecasting model. Bound.-Lay. Meteorol. 162, 117–142. https://doi.org/10.1007/s10546-016-0185-2.
Zhang, L., Li, Q.B., Gu, Y., Liou, K.N., Meland, B., 2013. Dust vertical profile impact on global radiative forcing estimation using a coupled chemical-transport–radiative-

transfer model. Atmos. Chem. Phys. 13, 7097–7114. https://doi.org/10.5194/acp-13-7097-2013.

Zhao, C., Chen, S., Leung, L.R., Qian, Y., Kok, J.F., Zaveri, R.A., Huang, J., 2013. Uncertainty in modeling dust mass balance and radiative forcing from size parameterization. Atmos. Chem. Phys. 13, 10733–10753. https://doi.org/10.5194/acp-13-10733-2013.

Zhao, C., Liu, X.H., Leung, L.R., Hagos, S.M., 2011. Radiative impact of mineral dust on monsoon precipitation variability over West Africa. Atmos. Chem. Phys. 11, 1879–1893. https://doi.org/10.5194/acp-1l-1879-2011.

Zhao, C., Liu, X.H., Leung, L.R., Johnson, B., McFarlane, S.A., Gustafson, W., Fast, J.D., Easter, R.C., 2010. The spatial distribution of mineral dust and its shortwave radiative forcing over North Africa: modeling sensitivities to dust emissions and aerosol size treatments. Atmos. Chem. Phys. 10, 8821–8838. https://doi.org/10.5194/acp-10-8821-2010.